

Creating rotational coherences in molecules aligned along the intermediate moment of inertia axis.

Emil J. Zak^{1,*}

¹*BEIT, Mogilska 43 31-545 Kraków, Poland* †

(Dated: November 21, 2022)

We propose and computationally study a method for simultaneously orienting the angular momentum of asymmetric top molecules along: 1) a laboratory-fixed direction; 2) the molecular intermediate moment of inertia axis; 3) the laser field wavevector. For this purpose we utilize a coherent control scheme in which a tailored-pulse optical centrifuge populates rotational states with well defined projections of the total angular momentum onto molecular axes. Appropriately time-shaped optical centrifuge pulses can leave the rotational wavepacket in peculiar rotational coherences which lead to a good degree of 3-dimensional transient alignment, with an arbitrary molecular axis pointing along the laser pulse propagation direction. As an example, we demonstrate how to generate highly resilient rotational quantum states of D₂S in which the molecule rotates mainly about its intermediate inertia axis, such that its electric dipole moment is permanently aligned along the propagation direction of the laser pulse. Applications might include accessing less obscured information in various photo-electron imaging experiments.

I. INTRODUCTION

For gaining direct access into the physics in the molecular frame, it is imperative to maximally confine at least one of the molecule's axes along a laboratory-fixed direction. Experiments utilizing high-harmonic generation (HHG) [1–7], laser-induced electron diffraction (LIED) [8–12], direct photo-electrons [13–25] or X-ray diffraction [26, 27] have been successfully used to probe the structure and ultra-fast dynamics of the gas phase molecules.

However, direct application of these techniques to randomly oriented gas phase molecular samples has limited use, due to the averaged-response from all possible laboratory-frame orientations. Information about the structure and dynamics of molecular systems obtained from randomly oriented samples is therefore obscured and requires special algorithms [1, 2, 28] to be reliably retrieved. For this reason, several techniques for determining the molecular structure and dynamics at high temporal and/or spatial resolution [29–38] have greatly benefited from pre-aligning the molecular samples in one [4, 7, 13, 15, 37, 39–43], two [44–46], and three [47–53] spatial directions. Applications of molecular alignment have also been found in stereodynamical control of chemical reactions [54–57].

Molecular alignment of linear and symmetric top molecules in 1-D is routinely performed at high efficiency with strong laser pulses [42, 58–60, 60–66]. However, the majority of molecules with more than two atoms are asymmetric tops, such as water, to mention one. For most imaging experiments it is highly desirable to have the molecule aligned, even transiently, in space free of any

fields but the probe, to avoid interference of the aligning field with the probe field. The typically used for this purpose impulsive alignment [50, 67–70] approach aims at creating a broad rotational population distribution and a locked-phase relation between the wavepacket components.

Field-free alignment through an impulsive or mixed-field excitation [71–73] proves inherently burdened for asymmetric top molecules [1, 74–77]. A reason for this are three different moments of inertia along the principal inertia axes, which give incommensurable frequencies between different rotational quantum states; their quantum rotational dynamics is chaotic, meaning the well known perfect quantum revivals observed for symmetric tops are no longer achievable [1, 53, 74–76]. As there is no obvious mitigation to this problem, experiments [1, 2] have aimed at kicking the asymmetric top molecule with an ultra-short intense non-resonant laser pulse and decomposing the measured response onto the three perpendicular principal inertia axis contributions - usually very low degrees of transient alignment of smallest, middle or largest moment of inertia axis have been observed [47, 50, 78–81].

Mastering the alignment of the smallest (*a*-), middle (*b*-) and largest (*c*-) polarisability axis along a laboratory-fixed direction would open a vast field of possibilities for imaging the molecular-frame dynamics, with direct tomography of molecular orbitals [1, 30, 38, 82, 83] as an example.

Three major types of molecular axis alignment (angular momentum orientation) are shown in Fig. 1. On the example of a bent triatomic molecule, Fig. 1 displays possible orientations of the molecular polarisability axis with respect to the laboratory *Z*-direction: *syn* (*a*-axis aligned with *Z*), *anti* (*b*-axis aligned with *Z*) and *gauche* (*c*-axis aligned with *Z*). In the *syn* and *gauche* case, the intermediate polarisability axis (to a good approximation the intermediate inertia axis, very often also the dipole moment) of the molecule rotates in the plane of the confining field, whereas in the *anti* orientation, the

* emil@beit.tech

† Former affiliation: Center for Free-Electron Laser Science, Deutsches Elektronen-Synchrotron DESY, Notkestraße 85, 22607 Hamburg, Germany

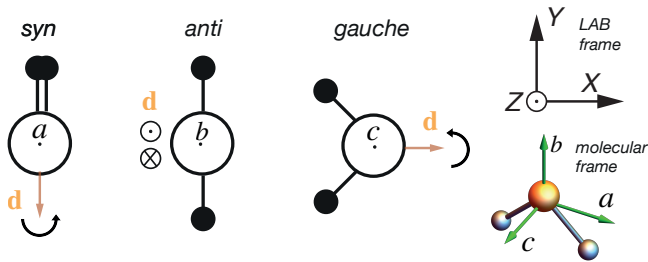


Figure 1. Schematic view of an asymmetric top molecule rotating about its a -, b - and c - principal inertia axis. From the laboratory frame perspective the molecules are in *syn*, *anti* and *gauche* geometry. We assume that the probe pulse propagates along the laboratory Z -direction, whereas the molecule-confining pulse is restricted to the XY plane. d denotes the dipole moment vector.

dipole moment permanently points along the wavevector of the confining field (Z -direction). A missing piece to complete the picture of molecular alignment geometries is placing the symmetry axis, or more generally the intermediate inertia b -axis of an asymmetric top molecule, along the probe pulse's wave-vector; i.e. achieving the *anti* alignment shown in Fig. 1. Such an alignment is complementary to the a - and c -axis alignments.

Whereas the entire class of impulsive and mixed-field alignment techniques rely on strong confinement of the spatial observables, at the cost of high uncertainty in the angular momentum, an alternative approach of the angular momentum orientation [84–87] utilizes a reversed principle. It gives up spatial confinement in two directions (x, y), to strongly orient the angular momentum z -component J_z and the z -axis along the same laboratory-frame direction. An advantage carried by large magnitude and strongly oriented angular momentum samples is their stability and high resistance to collisional decoherence for up to microseconds [88–91]. Such resilient molecular gyroscopes can have either their largest- or smallest-electronic polarisability axis aligned with the polarisation plane of the confining electric field [46, 92, 93].

So far, alignment of the intermediate (b -) polarisability axis have remained elusive both theoretically and experimentally. None of available impulsive or adiabatic alignment or angular momentum orientation techniques were proposed to realize the *anti* geometry from Fig. 1. This is because the rotation about the intermediate axis (b -rotation) is quite different from the other two rotations, both classically and quantum-mechanically.

Classically the b -rotation is unstable, with the molecule (object) flipping its orientation periodically [94–98], which is also known as the tennis racket theorem or the Dzhabenikov effect [96, 98]: the intermediate axis lies on the phase-space separatrix between two stable points of a - and c - rotation.

Quantum mechanically, the situation is quite different. First, as long as no parity-breaking interaction is present, the molecule may only be aligned along with the external

field, such that no preferable orientation is distinguished. In this sense, the flipping-rotation known from classical physics is inherently present in the quantum wavefunction. Secondly, rotational states attributed to the rotation about the b -axis are located in the middle of the rotational energy levels manifold, making it cumbersome to access via optical methods (see Fig. 2), in contrast to accessing the a - or c - rotating states. So far, there have been no reports of a coherent optical excitation targeting these b -rotation states.

In this work, we show how to control the rotation axis of asymmetric top molecules simultaneously in the laboratory-frame and in the molecular-frame, with the classically unstable axis of rotation aligned with the laser field wave-vector.

First we computationally identify and characterize rotational states of asymmetric top molecules, which can be associated with the rotation about the intermediate inertia axis (b -rotation states); they lie in the middle of the rotational energy levels manifold. Next, we utilize a modification of the optical centrifuge technique already introduced in Ref. [99] to show how the b -rotation states can be efficiently populated in the asymmetric top D_2S molecule. Appropriate timing of the centrifuge pulse creates arbitrary coherences between the stationary b -axis rotating states, some of which exhibit classical-like rotational motion [100, 101] and a fair degree of 3D alignment, in field-free conditions. A new type of rotational transient, *B-type*, is discussed.

The results presented in this work, together with the results of Ref. [92] complete the study of 1D- and 3D-alignment of asymmetric top molecules (through angular momentum orientation), with either of their a -, b - or c - polarisability axis pointing along the wavevector of the probing pulse [45, 102]. In principle, complete molecular-frame information could be collected in an imaging experiment combined with the technique described below.

II. PRINCIPAL ROTATION STATES OF D_2S

Fig. 2 displays a schematic of rotational energy levels of the D_2S molecule with low total angular momentum. For any value of the rotational quantum number J there is a multiplet of $2J + 1$ levels, which are colored according to the average values of the angular momentum projection operators onto the D_2S 's principal axes of inertia $\langle \hat{J}_a^2 \rangle$ (cyan color), $\langle \hat{J}_b^2 \rangle$ (yellow color), and $\langle \hat{J}_c^2 \rangle$ (purple color). A continuous map covering all possible angular momentum projections is shown in the triangle in the inset to Fig. 2.

Highest-energy levels at each total angular momentum J correspond to $\langle \hat{J}_a^2 \rangle \approx J^2$ (cyan color), i.e., in these states the molecule rotates about the a -axis and $K_a = J$ becomes a near-good quantum number, denoting the projection of the total angular momentum onto the a principal-inertia-axis. Such state can be dubbed a *prin-*

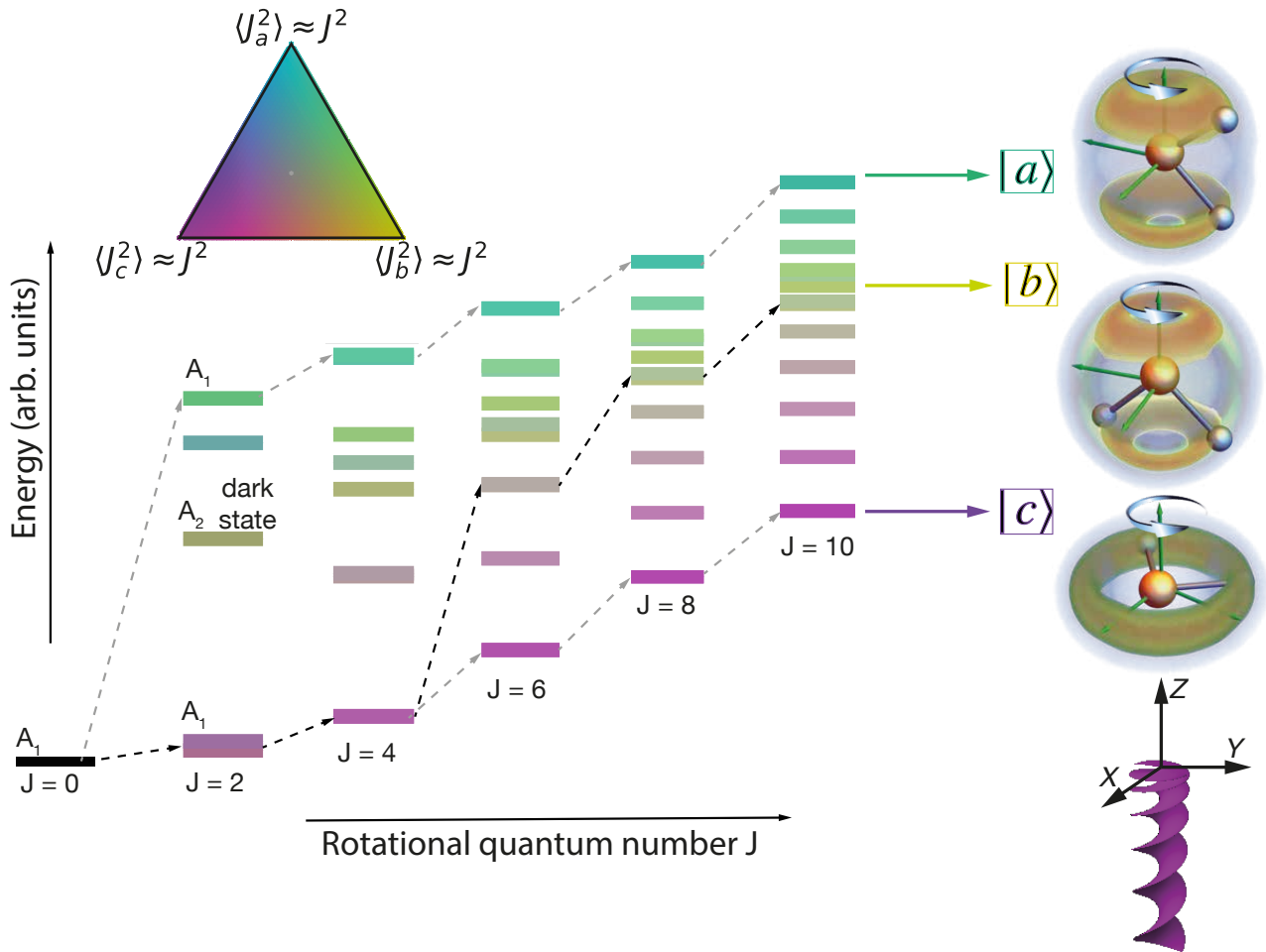


Figure 2. Rotational energy levels of D_2S and a selected rotational excitation path leading to the principal rotation b -states $|b\rangle$ marked with dashed black arrows. For any value of the rotational quantum number J there is a multiplet of $2J + 1$ levels, which are colored according to the average values of the angular momentum projection operators onto the D_2S 's principal axes of inertia $\langle J_a^2 \rangle$ (cyan color), $\langle J_b^2 \rangle$ (yellow color), and $\langle J_c^2 \rangle$ (purple color). A continuous map covering all possible angular momentum projections is shown in the triangle in the inset. Right panel shows 3D probability densities for finding deuterium nuclei in three different principal rotation states ($|a\rangle$, $|b\rangle$ and $|c\rangle$). The laboratory frame and a schematic of an optical centrifuge pulse are shown in the bottom right corner.)

principal rotation state and marked with $|a\rangle$. Similarly, the lowest-energy levels correspond to rotation about the c -axis with $K_c = J$ (purple color), while those with energies in the middle are mixtures of rotations about different axes with some of them exhibiting classically unstable b -axis rotation (yellow color).

In the right panel in Fig. 2 shown are the calculated 3D probability densities for the deuterium atoms for the highest-, middle-, and lowest-energy levels at $J = 10, M = 10$. Here, M is the quantum number for the Z -component of the angular momentum operator in the laboratory-fixed frame, which is shown in the bottom right corner, together with an optical centrifuge pulse. A non-resonant rotational excitation leading to the population of principal rotation states $|a\rangle$, $|b\rangle$ or $|c\rangle$ can be realized by the interaction with linearly polarized light with accelerated rotation of its polarization plane, known

as an optical centrifuge [46, 92, 93]. Interaction of the electronic polarisability with the centrifuge pulse promotes only transitions with $\Delta J = 2$ and $\Delta M = \pm 2$, depending on the handedness of the centrifuge pulse. Lowest rotational energy excitation path (c -path marked with thin gray arrows in Fig. 2) proceeds in near-oblate asymmetric top molecules, such as D_2S , at low acceleration rates of the optical centrifuge pulse, as discussed in Ref. [92]. High acceleration rates of the centrifuge field populate predominantly states along the highest excitation path (a -path). In near-prolate molecules, populating states along the c -path requires appropriate modulation of the centrifuge's field intensity [93].

III. POPULATING B-PRINCIPAL ROTATION STATES WITH AN OPTICAL CENTRIFUGE

A proposition to coherently populate $|b\rangle$ principal rotation states has been so far lacking. Here we propose how to use the optical centrifuge to populate the $|b\rangle$ states. Because such an excitation cannot come directly through the $|J = 0, M = 0, +\rangle \rightarrow |J = 2_{K_b \approx 2}, M = 2, +\rangle$ transition, as the upper state has A_2 symmetry, which in the absence of parity-breaking (electric dipole) interaction remains dark, another excitation path must be found. For this purpose we utilized a shortest path finding algorithm [99] to determine an optimal excitation pathway (based on largest overall transition moment) connecting the ground state with a $|b\rangle$ -state at $J = 14, M = 14$. Initial part of this path is shown in Fig. 2 with thick black dashed arrows and it reads $|J, M, h, \tau\rangle$:

$$\begin{aligned} |0, 0, 1, +\rangle &\rightarrow |2, 2, 1, +\rangle \rightarrow |4, 4, 1, +\rangle \rightarrow |6, 6, 5, +\rangle \rightarrow \\ |8, 8, 9, +\rangle &\rightarrow |10, 10, 13, +\rangle \rightarrow |12, 12, 17, +\rangle \rightarrow |14, 14, 21, +\rangle \end{aligned} \quad (1)$$

where h labels the rotational states in ascending energy order for each J , whereas τ is the rotational parity. With the rotational excitation path selected, the optical centrifuge pulse envelope has to be modulated to reach significant intensities near the times at which the pulse's instantaneous frequency matches resonance with the rotational transition. The intensity envelope of the centrifuge pulse has been modeled with *sinc* functions centered at appropriate resonance times determined by the centrifuge's acceleration rate β . Such tailoring of the centrifuge's pulse intensity is quite universal, so that both near-prolate molecules and near-oblate molecules can be efficiently excited into their b -rotation states. Intensity-modulated pulse profiles can now be created with the use of a 4-f pulse shaper combined with a standard centrifuge setup [103].

The time-dependent Schrödinger equation has been solved on a grid of the centrifuge parameters: field strength E_0 , width of sinc function σ and acceleration rate β to find optimal and robust values: $E_0 = 1.7 \cdot 10^8$ V/cm, $\sigma = 7$ ps and $\beta = 60$ GHz/ps, which guarantee good excitation efficiency. The rotational-dynamics calculations of D_2S were performed in two steps. First, energies and their transition moments were obtained with the full-dimensional variational procedure TROVE [104–106] together with a highly-accurate spectroscopically adjusted potential energy surface [107] and a high-level *ab initio* polarizability surface [93] of the H_2S molecule within the Born-Oppenheimer approximation. In the second step, the time-dependent solutions for the full molecule-field interaction Hamiltonian were obtained using the computational approach Richmol [108, 109] in the field-free basis. The wavefunctions were time-propagated using the split-operator method with a timestep of 10 fs. The time-evolution operator was evaluated using an iterative procedure based on the Krylov subspace methods.

Fig. 3 displays time-profiles of rotational state populations of D_2S along the selected b -rotation excita-

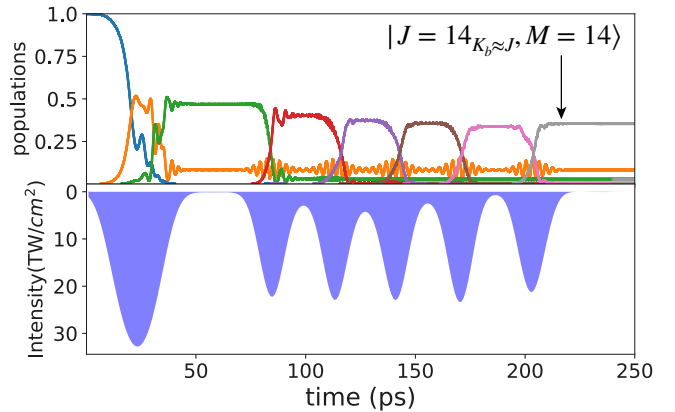


Figure 3. Time-profiles of D_2S rotational states' populations along the excitation path given in Equation 1 leading to a b -principal rotation state. Bottom panel: intensity profile of the centrifuge pulse. Target state $|J = 14_{K_b \approx J}, M = 14\rangle$ is marked with an arrow.

tion path given in Equation 1. Starting from the rotational ground state (see Fig. 2), the excitation proceeds at a good yield ($\approx 35\%$) up to the target state $|J = 14_{K_b \approx J}, M = 14\rangle$. Bottom panel in Fig. 3 shows the intensity profile of the centrifuge pulse. The major source of population losses occurs at the initial forking stage $J = 0, M = 0 \rightarrow J = 2, M = 2$. The efficiency can be enhanced by lowering the centrifuge's acceleration rate, at the cost of a longer pulse.

IV. PROPERTIES OF B-PRINCIPAL ROTATION STATES

Fig. 4 depicts 3D probability distributions for the molecular-frame rotation axes of D_2S , plotted for three different $|b\rangle$ -principal rotation states. The rotational states are denoted as $|J_{k_b \approx J}, M, h, \tau\rangle$, with h labelling energy levels in ascending order for each J -multiplet, and τ is parity. We selected a representative $|b\rangle$ -principal rotation state $|20_{k_b \approx 20}, 20, 25, +\rangle$ shown in the left panel in Fig. 4 to demonstrate how the rotation-axis probability density is localized near the b -axis.

The degree of 1D alignment of the rotation axis along the b -axis is similar for all $|b\rangle$ principal rotation states and reads $\langle \cos^2 \theta_{bZX} \rangle \approx 0.93$, with little sensitivity to J . The $|b\rangle$ states can be found up to high values of the total angular momentum J , with $|58_{k_b \approx 58}, 58, 68, +\rangle$ state shown in the middle panel in Fig. 4. This state exhibits a sharp maximum probability which splits into two poles located on opposite sides of the b -axis, at $\theta = 9.1^\circ, \phi = 90.5^\circ, 269.7^\circ$ and $\theta = 170.1^\circ, \phi = 90.5^\circ, 269.7^\circ$. The degree of alignment for the $|58_{k_b \approx 58}, 58, 68, +\rangle$ state measured along the b -axis reads $\cos^2 \theta_{bZX} = 0.91$. The sharpening of the 3D rotation axis probability maximum with increasing J does not necessarily translate into higher degrees of alignment, due to emergence of new probability

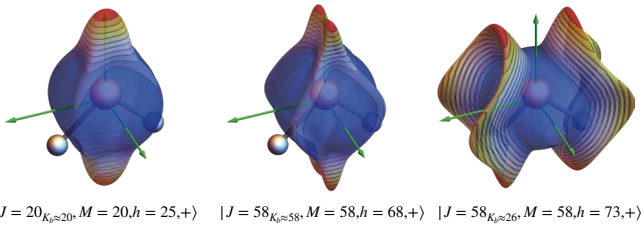


Figure 4. 3D probability distributions for the molecular-frame rotation axes of D_2S , plotted for three different $|b\rangle$ -principal rotation states. $|J_{k_b}, M, h, \tau\rangle$ denotes the rotational state with h labelling energy levels in ascending order for each J -multiplet, and τ is parity. $M = J$ implicitly. Green axis system denotes the molecular principal inertia frame.

islands related to rotational energy level clustering. This clustering effect causing rearrangement of rotation axis has been discussed elsewhere [93, 99].

Interestingly some cluster states located near the middle of a given J -rotational energy manifold have their probability density for the rotation axis lying close to the classical separatrix [94–98] between the a - and c -stable rotation, as the one shown in the right panel in Fig. 4. The probability for the axis of rotation is then delocalized along a well defined path connecting opposite orientations of the molecule. Classically, rotation of the molecule about a - or c -axis or near these axes features stable *oscillating* or *rotating* trajectories [97] of the molecule-fixed angular momentum. Rotation axis initially placed near the b -axis is unstable, showing periodic flipping, whose period is sensitive to the initial conditions. This latter behavior is known as the *tennis racket effect* [94–98]. Quantum mechanically, the stationary $|a\rangle$, $|b\rangle$ or $|c\rangle$ states have an unchanged probability density as well as both orientations are equivalent, such that axis flipping is inherent. Orientation of such states is difficult via the interaction with the electric dc field due to large energy separation between opposite parity pairs (A_1/A_2).

One can create transient orientation of principal rotation states through coherent superposition of opposite parity states, for instance: $|A_1\rangle + e^{-i\Delta E/\hbar t}|A_2\rangle$, in which the frequency of the dipole moment vector flipping equals the energy ΔE separating the $|A_1\rangle, |A_2\rangle$ states. If this separation is large, the oscillations are very fast. We observe that all types of principal rotation states, that is $|a\rangle$, $|b\rangle$ and $|c\rangle$ have their respective $|A_1\rangle$ counterparts located within several wavenumbers, such that a unidirectionally rotating and oriented states can in principle be created. However in the field-free case, all such wavepackets will exhibit flipping of the dipole moment at a rate given by the energy splitting between the $|A_1\rangle, |A_2\rangle$ states. In this sense, the tennis racket effect is present in all quantum rotational states. Another possibility is to use a strong dc field to create orientation, in which case it is possible to create $|A_1\rangle \pm |A_2\rangle$ field-dressed states with locked phase between its components, such that the molecule is ori-

ented up or down, respectively. Such orientation lasts as long as the field is present. Very strong dc electric fields up to few MV/cm are needed to achieve orientation this way.

V. COHERENCES BETWEEN PRINCIPAL ROTATION STATES: ROAD TO 3D ALIGNMENT

As shown in Fig. 3, appropriate turn-off time of the centrifuge pulse can leave the wavepacket in a coherence between neighboring J and $J + 2$ rotational states. An interesting characteristic of such two-state wavepackets is a classical-like (cogwheel) rotation of the rotational probability density [100, 101]. Interference between the $|b_J\rangle$ and $|b_{J+2}\rangle$ state spawns a well localized nuclear density, which revolves about the b -axis at a constant frequency determined by the energy difference between the composing states. Fig. 5 displays four snapshots of such a probability density for the deuterium atoms in D_2S for the $\frac{1}{\sqrt{2}}(|10, k_b \approx 10, 10, +\rangle + e^{-i\omega t}|12, k_b \approx 12, 12, +\rangle)$ coherence. The classical-like rotation period decreases linearly with the total angular momentum J and for the $J = 10, 12$ pair it is $T = 154$ fs which corresponds to 216 cm^{-1} energy separation between states composing the cogwheel wavepacket.

Effectively, the cogwheel wavepackets feature highly oriented angular momentum along the molecule-fixed z -axis and the laboratory-fixed Z axis as well as a degree of molecular-axis localization in the plane perpendicular to the angular momentum: the xy and XY plane. The degree of 3D alignment in a cogwheel principal rotation state can be measured with the 2D alignment cosines of respective molecular axes onto the laboratory XZ and XY planes, which in the case of wavepacket from Fig. 5 are given by: $\langle \cos^2 \theta_{bZX} \rangle = 0.71 - 0.81$, $\langle \cos^2 \theta_{cZX} \rangle = 0.18 - 0.4$, $\langle \cos^2 \theta_{cXY} \rangle = 0.28 - 0.73$.

Both the probability densities shown in Fig. 5 and the alignment cosines were calculated using monte-carlo sampling (1 Million points) of the rotational wavefunction. We must note here that D_2S , which has been chosen for computational convenience, is a molecule with very large rotational constants ($A = 164.57 \text{ GHz}$, $B = 135.38 \text{ GHz}$, $C = 73.24 \text{ GHz}$) [110], meaning that the rotational dynamics is also relatively fast. Heavier rotors, such as SO_2 or benzene derivatives have their cogwheel-rotation-period in the range of several picoseconds.

The probability density for finding the deuterium atoms in 3D space in a cogwheel $J, J+2$ state, such as the one depicted in Fig. 5, can be written as:

$$\rho_J(\theta, \phi, \chi, t) = N \cos^{4J} \frac{\tilde{\theta}}{2} \left[2J + 1 + (2J + 5) \cos^8 \frac{\tilde{\theta}}{2} + 2\sqrt{2J + 5} \cos \left(\Delta J(\tilde{\phi} + \tilde{\chi}) - \omega t \right) \right] \quad (2)$$

where $\tilde{\theta} = \theta - \theta_D$, $\tilde{\phi} = \phi - \phi_D$ and $\tilde{\chi} = \chi - \chi_D$ are the

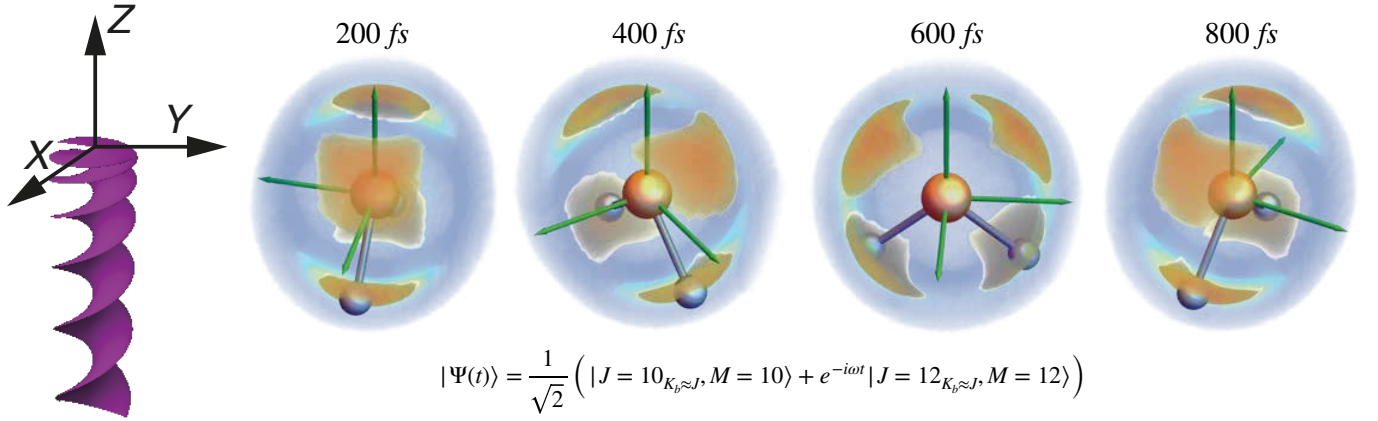


Figure 5. Snapshots of 3D probability density of the deuterium atoms in a *cogwheel state* of D_2S : $\frac{1}{\sqrt{2}} (|10, k_b \approx 10, 10, +\rangle + e^{-i\omega t} |12, k_b \approx 12, 12, +\rangle)$. Transient 3D alignment is visible. In the left panel the XYZ laboratory-frame is marked together with the centrifuge pulse. The period of rotation for this state is $T = 154fs$.

Euler angles denoting the position of deuterium atoms in D_2S , in bisector molecular-frame embedding, i.e. where the b -axis lies along the molecule-fixed z -axis. N is the normalization constant.

The functional form of the cogwheel probability density shown in (2) suggests that cogwheel states have at most two effective degrees of rotational freedom: $\theta, \phi + \chi$ and that the nuclear density rotates about the molecule-fixed z - and laboratory-fixed Z -axis at a frequency ω . In eq.(2) $\Delta J = 2$, such that the cogwheel has two 'teeth', which also fixes the maximum degree of transient 3D alignment to $\langle \cos^2 \theta_{aXY} \rangle = \langle \cos^2 \theta_{cXY} \rangle = 0.73$, $\langle \cos^2 \theta_{bXZ} \rangle = 0.93$.

A higher degrees of field-free alignment could be achieved if one created a coherent wavepacket in which one molecular axis is strongly confined to the laboratory Z -axis, while the wavefunction projected onto the plane perpendicular to Z produced constructive interference at given rotational revival times. Such a scenario is possible with a coherence between several principal rotation states a -, b - or c -, as written in the equation below:

$$\begin{aligned} \psi(t) &= \sum_{J=J_{min}}^{J_{max}} c_J |J_{K_\lambda \approx J}, M = J, h_J, \tau\rangle \approx \\ &\approx \sum_{J=J_{min}}^{J_{max}} |c_J| e^{-i(\Delta J(\phi+\chi) - E_J t + \phi_J^0)} \cos^2 J \frac{\theta}{2} + h.c. \end{aligned} \quad (3)$$

where $\lambda = a, b$ or c . Here ϕ_J^0 is the static phase of the c_J complex coefficient and $\Delta J = 2$ denotes the difference in the total angular momentum between states in the wavepacket.

The idea behind the wavepacket shown in (3) is to create rotational transients [78–81, 111–113], in the coherent superposition of the principal rotation states. The alignment cosine measuring the degree of alignment in the laboratory XY plane with respect to the X -axis can

be calculated analytically for the coherence given in (3):

$$\langle \cos^2 \phi \rangle_{\psi(t)} = \sum_{J=J_{min}}^{J_{max}-2} g_J \cos(\omega_{J+2J} t + \Delta \phi_{J+2J}^0) \quad (4)$$

where $g_J = \frac{1}{4J+6} |c_J| |c_{J+2}| \sqrt{(2J+1)(2J+5)}$. In derivation of (4) we assumed that $K_\lambda = J$, and that $\lambda = a, b$ or c is the molecule-fixed z -axis. Full expression for the alignment cosine, in a non-perfect principal rotation state is given in Section VI.

From the form of the wavefunction given in (3) we infer that the degree of alignment of the molecular axis $\lambda = a, b$ or c along the laboratory-fixed Z -axis is high, depending which principal rotation state one pick: $|a\rangle$, $|b\rangle$ or $|c\rangle$, respectively. The other two molecular axes are confined to the XY plane and when the coherence given in (3) consists of more than two rotational states, the $\langle \cos^2 \phi \rangle_{\psi(t)}$ alignment cosine exhibits a revival pattern. This suggests that at certain times the degree of alignment with respect to the laboratory X -axis bound to reach maximum, leading to transient 3D alignment. To demonstrate this concept, we calculated the alignment cosines for the principal inertia axes of D_2S in the rotational state given in (3) with $J_{min} = 14$ and $J_{max} = 20$ for $\lambda = a$ and a high degree of 3D alignment was reached: $\langle \cos^2 \theta_{cXY} \rangle_{max} = \langle \cos^2 \theta_{bXY} \rangle_{max} = \langle \cos^2 \phi \rangle_{max} = 0.88$, $\langle \cos^2 \theta_{aXZ} \rangle_{max} = 0.94$, due to an A-transient [80, 113]. A flat relative-initial phase relation between the respective components was assumed. Interestingly, a choice of random phases also yields high degrees of maximum alignment, with $\langle \cos^2 \theta_{cXY} \rangle_{max} \approx 0.85$.

Generation of a C-type and most interestingly a B-type transient is depicted in Fig. 6, where time-profiles were calculated for appropriate 2D alignment cosines for three wavepackets, representing coherences between the a - (uppermost panel), b - (middle panel) and c - (bottom panel) principal rotation states in D_2S in the range $J = 14 - 20$ (see (3)).

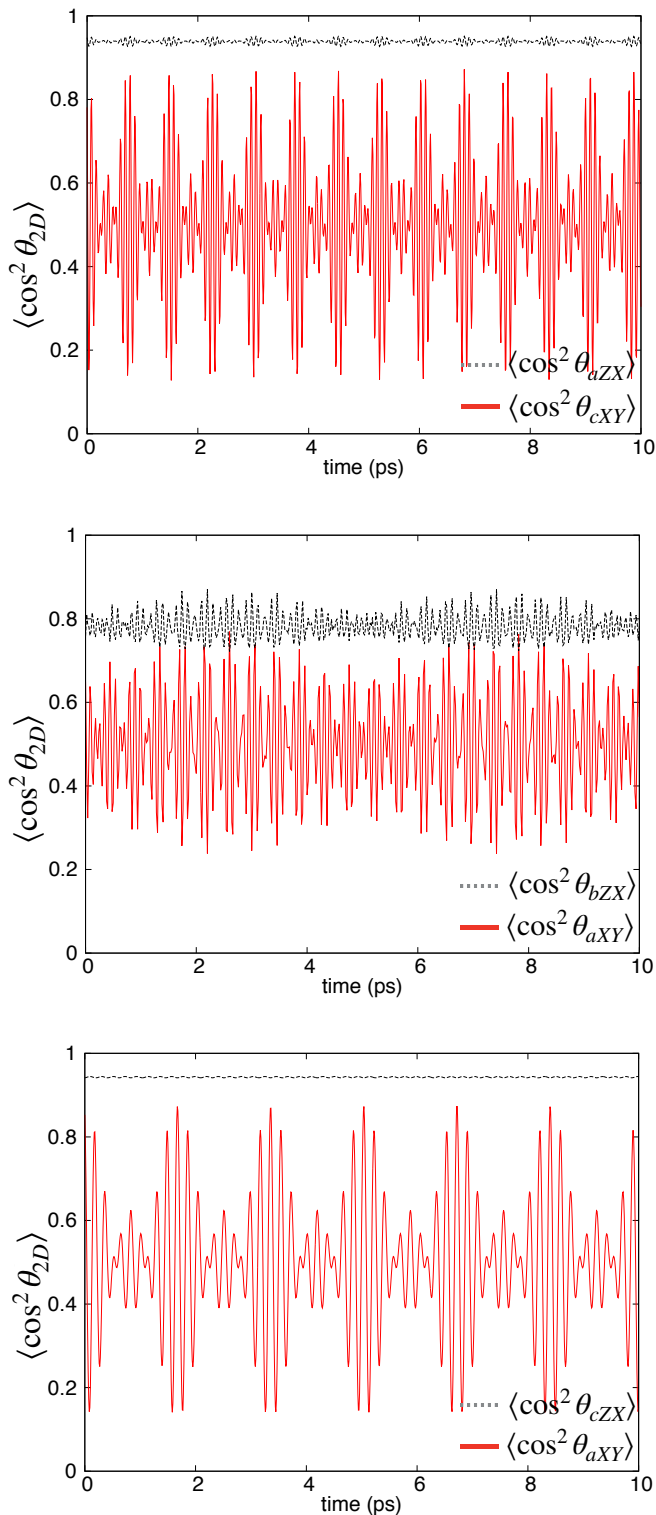


Figure 6. Calculated 2D alignment-cosine time-profiles for three wavepackets, representing coherences between the a - (uppermost panel), b - (middle panel) and c - (bottom panel) principal rotation states in D_2S in the range $J = 14 - 20$ (see (3)). The alignment cosines measure the degree of alignment of the principal axes of inertia of D_2S with respect to the laboratory axes. For instance $\langle \cos^2 \theta_{aZX} \rangle$ is the 2D alignment cosine calculated with respect to the laboratory Z axis of the projection of the molecular a axis onto the ZX detector plane. High degree of permanent 1D alignment is visible as well as sharp revivals of 3D alignment are present in all three cases.

The top panel shows how the $\langle \cos^2 \theta_{aXZ} \rangle(t)$ alignment cosine maintains a high value of about 0.94 while the $\langle \cos^2 \theta_{cXY} \rangle$ alignment cosine has periodic maxima, reaching up to 0.88. Similarly the bottom panel in Fig. 6 shows how the c -principal inertia axis is confined to the laboratory Z axis ($\langle \cos^2 \theta_{cZX} \rangle_{max} = 0.94$) and the a -axis shows signs of transient alignment along the X axis ($\langle \cos^2 \theta_{aXY} \rangle_{max} = 0.87$).

In the middle panel in Fig. 6 we can see a new type of transient [80, 113]: the B-type, which corresponds to $\Delta J = 2$ and $\Delta K = 1$ coupling of rotational states ($|b\rangle \leftrightarrow |b'\rangle$). Coherences between the principal rotation $|b\rangle$ states reveal a fair transient degree of 3D alignment with $\langle \cos^2 \theta_{bZX} \rangle_{max} \approx 0.8$ and $\langle \cos^2 \theta_{aXY} \rangle_{max} \approx 0.78$. For consistency, we have not chosen for the middle panel in Fig. 6 a coherence between b -principal rotation states which produced highest possible degree of alignment (1D or 3D), but rather kept identical J -range ($J = 14 - 20$) across all panels.

A 3D alignment of molecular axes and 1D orientation of angular momentum, as shown in Fig. 6, can be generated with appropriately tailored optical centrifuge pulses, with the pulse area and timing calculated with the aid of coherent optimal control [114–116].

To summarize, we demonstrated the existence of rotational quantum states in asymmetric top molecules in which the rotation axis is nearly aligned with the intermediate inertia axis. We call them principal rotation states. In a computational study, an optical centrifuge technique was shown to efficiently populate a selected $|b\rangle$ principal rotation state, in which the angular momentum is fixed both along the laboratory-fixed Z axis and the molecular b -axis and along the laser field’s wavevector. Such an alignment is complementary to the previously considered alignments of the most- and least- polarisable molecular axis. Interestingly, in D_2S the b -alignment results in the molecule’s dipole moment permanently aligned with the wavevector of the confining field and of the following probe pulse, in some analogy to k -alignment introduced by Smeenk et. al. [44, 45]

Finally, we also presented a scheme allowing to achieve a good degree of transient 3D alignment, with an arbitrary molecular axis pointing along the laser field’s wavevector. The accompanying strongly oriented angular momentum of nearly arbitrary magnitude preserves the created coherence, in the same way as gyroscopes do, giving an elevated resilience to collisional decoherence, hence adding stability to the degree of alignment. Applications of the 3D a -, b - and c -alignment can enable access to less obscured information in various photo-electron imaging experiment [1, 30, 38, 83],

ACKNOWLEDGMENTS

I thank Jochen Küpper and Andrey Yachmenev for helpful discussions.

DISCLAIMER

Part of this manuscript has been written during the time of the author's stay at the Center for Free-Electron Laser Science, Deutsches Elektronen-Synchrotron DESY, although no part of this work has been created in the time of performing duties included in the author's employment contract. Therefore this work is not an official publication from the Center for Free-Electron Laser Science or the Deutsches Elektronen-Synchrotron DESY.

VI. APPENDIX A

Below a derivation is given of the equation for the alignment cosine from (4). We start with an even parity asymmetric top rotational state which has possibly maximal projection of the total angular momentum onto the quantization axis $\lambda = a, b$ or c :

$$\psi(t) = \sum_{J=J_{min}}^{J_{max}} c_J |J_{K\lambda \approx J}, M = J, h_J, \tau\rangle \quad (5)$$

where each contributing state is expanded in the symmetric-top basis:

$$|J_{K\lambda \approx J}, M = J, h_J, \tau\rangle = \sum_{K=0}^J a_K^{J, h_J, \tau} |J, K, M = J, \tau\rangle \quad (6)$$

and

$$|J, K, M, \tau\rangle = \frac{1}{\sqrt{2}} [|J, k, M\rangle + (-1)^\tau |J, -k, M\rangle] \quad (7)$$

with $|J, k, M\rangle = \sqrt{\frac{2J+1}{8\pi^2}} D_{MK}^{(J)*}(\theta, \phi, \chi)$ being the standard symmetric-top wavefunctions. Note that the value of K_λ in (5) depends on the molecular-frame embedding. We choose $\lambda = z$, such that $K_\lambda \approx J$ for $\lambda = a, b, c$. Then approximately one can write $|J_{K\lambda \approx J}, M = J, h_J, \tau\rangle \approx |J, K = J, M = J, \tau\rangle$ as the $a_K^{J, h_J, \tau}$ coefficient in (6) dominates. After short algebra we find an explicit form of the asymmetric top wavefunction as

$$\psi(t) = \frac{1}{4\pi} \sum_{J=J_{min}}^{J_{max}} \sqrt{2J+1} c_J e^{-i\phi J} \sum_{K=0}^J a_K^{J, h_J, \tau} \times \left[e^{-iK\chi} d_{JK}^J(\theta) + (-1)^\tau e^{iK\chi} d_{J, -|K|}^J(\theta) \right] \quad (8)$$

where we note that the expansion coefficients c_J are time-dependent and complex and can take the form: $c_J = |c_J| e^{-i(E_J t + \phi_J^0)}$, where ϕ_J^0 is the static phase of component state $|J_{K\lambda \approx J}, M = J, h_J, \tau\rangle$ and E_J is the energy of state.

The alignment cosine measuring the degree of alignment with respect to the X axis in the laboratory frame is given by

$$\langle \cos^2 \phi \rangle_{\psi(t)} = \langle \psi(t) | \cos^2 \phi | \psi(t) \rangle \quad (9)$$

where $\phi \in [0, 2\pi)$ is the polar Euler angle in the XY plane. With the wavefunction given in (8) the alignment cosine from (9) can be further written as

$$\langle \cos^2 \phi \rangle_{\psi(t)} = \frac{1}{16\pi^2} \sum_{J, J'=J_{min}}^{J_{max}} c_J^* c_{J'} \sqrt{(2J+1)(2J'+1)} \times \int_0^{2\pi} d\phi \cos^2 \phi e^{-i\phi \Delta J} \sum_{K, K'=0}^{J, J'} a_K^{J, h_J, \tau*} a_{K'}^{J', h_{J'}, \tau'} \times \int d\Omega \left[e^{-i\Delta - K\chi} d_{J'K'}^{J'} d_{JK}^J + e^{i\Delta - K\chi} d_{J', -K'}^{J'} d_{J, -K}^J + (-1)^\tau (e^{i\Delta + K\chi} d_{J', -K'}^{J'} d_{J, K}^J + e^{-i\Delta + K\chi} d_{J', K'}^{J'} d_{J, -K}^J) \right]$$

where $\Delta J = J' - J$, $\Delta_\pm K = K' \pm K$ and $d\Omega = \sin \theta d\theta d\chi$. Integrals over the ϕ angle impose rigorous selection rules on total angular momentum coupled by the $\cos^2 \phi$ operator:

$$\int_0^{2\pi} d\phi \cos^2 \phi e^{-i\phi \Delta J} = \begin{cases} 2 \frac{\sin(\pi \Delta J)}{\Delta J} \frac{\Delta J^2 - 2}{\Delta J^2 - 4} e^{-i\pi \Delta J}, & \text{if } \Delta J \neq 2 \\ \frac{\pi}{2}, & \text{if } \Delta J = 2 \end{cases} \quad (10)$$

we note that the integral given in (10) is non-zero only if $\Delta J = 2$. The integral over the χ Euler angle can also be

carried out analytically:

$$\int_0^{2\pi} d\phi e^{-i\phi \Delta_\pm K} = \begin{cases} -\frac{i}{\Delta_\pm K} (1 - e^{-i2\pi \Delta_\pm K}), & \text{if } \Delta_\pm K \neq 0 \\ 2\pi, & \text{if } \Delta_\pm K = 0 \end{cases} \quad (11)$$

whereas appropriate integrals over the azimuthal Euler angle θ are generally denoted as:

$$b_{JJ'KK'} = \int_0^\pi d\theta \sin \theta d_{JK}^J(\theta) d_{J', K'}^{J'}(\theta) \quad (12)$$

Equation (11) restricts contributions to the alignment cosine from states with the same K quantum number.

After some algebra one finds explicit expression for the

alignment cosine $\langle \cos^2 \phi \rangle_{\psi(t)}$:

$$\langle \cos^2 \phi \rangle_{\psi(t)} = \frac{1}{8} \sum_{J=J_{min}}^{J_{max}-2} |c_J| |c_{J'}| \sqrt{(2J+1)(2J+5)} \times \left[2b_{JJ+200}(1 + (-1)^J) \text{Re}(a_0^{J,h_J,\tau^*} a_0^{J+2,h_{J+2},\tau}) + \sum_{K \neq 0}^J \text{Re}(a_K^{J,h_J,\tau^*} a_K^{J+2,h_{J+2},\tau}) (b_{JJ+2KK} + b_{JJ+2-K-K}) \right] \cos(\omega_{J+2} t + \Delta\phi_{J+2}^0)$$

If we assume that only states with $K = J$ contribute significantly to the wavepacket, we arrive at the equation (4) from the main text, where we note

that $\text{Re}(a_J^{J,h_J,\tau^*} a_{J+2}^{J+2,h_{J+2},\tau}) \approx 1$, $d_{JJ}^J(\theta) = \cos^{2J} \frac{\theta}{2}$, $d_{J,-J}^J(\theta) = \sin^{2J} \frac{\theta}{2}$ and $b_{JJ+2JJ} = b_{JJ+2-J-J} = \frac{2}{2J+3}$.

- [1] L. Spector, M. Artamonov, S. Miyabe, T. Martinez, T. Seideman, M. Guehr, and P. Bucksbaum, Axis-dependence of molecular high harmonic emission in three dimensions, **5**, 3190 (2014).
- [2] R. M. Lock, S. Ramakrishna, X. Zhou, H. C. Kapteyn, M. M. Murnane, and T. Seideman, Extracting continuum electron dynamics from high harmonic emission from molecules, *Phys. Rev. Lett.* **108**, 133901 (2012).
- [3] R. Cireasa, A. E. Boguslavskiy, B. Pons, M. C. H. Wong, D. Descamps, S. Petit, H. Ruf, N. Thiré, A. Ferré, J. Suarez, J. Higuette, B. E. Schmidt, A. F. Alharbi, F. Légaré, V. Blanchet, B. Fabre, S. Patchkovskii, O. Smirnova, Y. Mairesse, and V. R. Bhardwaj, Probing molecular chirality on a sub-femtosecond timescale, *Nature Physics* **11**, 654 (2015).
- [4] M. D. Śpiewanowski and L. B. Madsen, Field-induced orbital distortion in high-order-harmonic generation from aligned and oriented molecules within adiabatic strong-field approximation, *Physical Review A* **89**, 10.1103/physreva.89.043407 (2014).
- [5] H. J. Wörner, J. B. Bertrand, D. V. Kartashov, P. B. Corkum, and D. M. Villeneuve, Following a chemical reaction using high-harmonic interferometry, *Nature* **466**, 604 (2010).
- [6] D. Baykusheva and H. J. Wörner, Chiral discrimination through bielliptical high-harmonic spectroscopy, **8**, 031060 (2018).
- [7] Y. He, L. He, P. Wang, B. Wang, S. Sun, R. Liu, B. Wang, P. Lan, and P. Lu, Measuring the rotational temperature and pump intensity in molecular alignment experiments via high harmonic generation, *Optics Express* **28**, 21182 (2020).
- [8] C. I. Blaga, J. Xu, A. D. DiChiara, E. Sistrunk, K. Zhang, P. Agostini, T. A. Miller, L. F. DiMauro, and C. D. Lin, Imaging ultrafast molecular dynamics with laser-induced electron diffraction, *Nature* **483**, 194 (2012).
- [9] P. B. Corkum and F. Krausz, *Attosecond Science*, **3**, 381 (2007).
- [10] M. Peters, T. T. Nguyen-Dang, E. Charron, A. Keller, and O. Atabek, Laser-induced electron diffraction: A tool for molecular orbital imaging, *Phys. Rev. A* **85**, 10.1103/physreva.85.053417 (2012).
- [11] C. D. Lin and J. Xu, Imaging ultrafast dynamics of molecules with laser-induced electron diffraction, *Physical Chemistry Chemical Physics* **14**, 13133 (2012).
- [12] R. Puthumpally-Joseph, J. Viau-Trudel, M. Peters, T. T. Nguyen-Dang, O. Atabek, and E. Charron, Laser-induced electron diffraction: inversion of photo-electron spectra for molecular orbital imaging, *Molecular Physics* **115**, 1889 (2017).
- [13] A. Trabattoni, J. Wiese, U. De Giovannini, J.-F. Olivieri, T. Mullins, J. Onvlee, S.-K. Son, B. Frusteri, A. Rubio, S. Trippel, and J. Küpper, Setting the photoelectron clock through molecular alignment, **11**, 2546 (2020), arXiv:1802.06622 [physics].
- [14] R. Johansen, K. G. Bay, L. Christensen, J. Thøgersen, D. Dimitrovski, L. B. Madsen, and H. Stapelfeldt, Alignment-dependent strong-field ionization yields of carbonyl sulfide molecules induced by mid-infrared laser pulses, **49**, 205601 (2016).
- [15] V. Kumarappan, L. Holmegaard, C. Martiny, C. B. Madsen, T. K. Kjeldsen, S. S. Viftrup, L. B. Madsen, and H. Stapelfeldt, Multiphoton electron angular distributions from laser-aligned CS₂ molecules, *Phys. Rev. Lett.* **100**, 093006 (2008).
- [16] K.-J. Yuan and A. D. Bandrauk, Above-threshold ionization in molecules by intense multiple-frequency circularly polarized laser pulses, *Physical Review A* **98**, 10.1103/physreva.98.023413 (2018).
- [17] A. N. Artemyev, A. D. Müller, D. Hochstuhl, and P. V. Demekhin, Photoelectron circular dichroism in the multiphoton ionization by short laser pulses. i. propagation of single-active-electron wave packets in chiral pseudopotentials, *The Journal of Chemical Physics* **142**, 244105 (2015).
- [18] A. D. Müller, A. N. Artemyev, and P. V. Demekhin, Photoelectron circular dichroism in the multiphoton ionization by short laser pulses. II. three- and four-photon ionization of fenchone and camphor, *The Journal of Chemical Physics* **148**, 214307 (2018).
- [19] A. D. Müller, E. Kutscher, A. N. Artemyev, and P. V. Demekhin, Photoelectron circular dichroism in the multiphoton ionization by short laser pulses. III. photoionization of fenchone in different regimes, *The Journal of*

Chemical Physics **152**, 044302 (2020).

- [20] C. S. Lehmann, N. B. Ram, I. Powis, and M. H. M. Janssen, Imaging photoelectron circular dichroism of chiral molecules by femtosecond multiphoton coincidence detection, *The Journal of Chemical Physics* **139**, 234307 (2013).
- [21] P. V. Demekhin, A. N. Artemyev, A. Kastner, and T. Baumert, Photoelectron circular dichroism with two overlapping laser pulses of carrier frequencies ω and 2ω linearly polarized in two mutually orthogonal directions, *Physical Review Letters* **121**, 10.1103/physrevlett.121.253201 (2018).
- [22] F. Brauße, G. Goldsztejn, K. Amini, R. Boll, S. Bari, C. Bomme, M. Brouard, M. Burt, B. Cunha de Miranda, S. Düsterer, B. Erk, M. Géléoc, R. Geneaux, A. S. Gentleman, R. Guillemin, I. Ismail, P. Johnsson, L. Journel, T. Kierspel, H. Köckert, J. Küpper, P. Lablanquie, J. Lahl, J. W. L. Lee, S. R. Mackenzie, S. Maclot, B. Manschwetus, A. S. Mereshchenko, T. Mullins, P. K. Olshin, J. Palaudoux, S. Patchkovskii, F. Penent, M. N. Piancastelli, D. Rompôtis, T. Ruchon, A. Rudenko, E. Savelyev, N. Schirmel, S. Techert, O. Travnikova, S. Trippel, J. G. Underwood, C. Vallance, J. Wiese, M. Simon, D. M. P. Holland, T. Marchenko, A. Rouzée, and D. Rolles, Time-resolved inner-shell photoelectron spectroscopy: From a bound molecule to an isolated atom, *Phys. Rev. A* **97**, 043429 (2018).
- [23] A. Kastner, T. Ring, H. Braun, A. Senftleben, and T. Baumert, Observation of photoelectron circular dichroism using a nanosecond laser, *ChemPhysChem* 10.1002/cphc.201900289 (2019).
- [24] T. Bayer, D. Gräffing, S. Kerbstadt, D. Pengel, K. Eickhoff, L. Englert, and M. Wollenhaupt, Time-resolved 3D imaging of ultrafast spin-orbit wave packet dynamics, **21**, 033001 (2019).
- [25] A. Kastner, G. Koumarianou, P. Glodic, P. C. Samartzis, N. Ladda, S. T. Ranecky, T. Ring, S. Vasudevan, C. Witte, H. Braun, H.-G. Lee, A. Senftleben, R. Berger, G. B. Park, T. Schäfer, and T. Baumert, High-resolution resonance-enhanced multiphoton photoelectron circular dichroism, *Physical Chemistry Chemical Physics* **22**, 7404 (2020).
- [26] T. Kierspel, A. Morgan, J. Wiese, T. Mullins, A. Aquila, A. Barty, R. Bean, R. Boll, S. Boutet, P. Bucksbaum, H. N. Chapman, L. Christensen, A. Fry, M. Hunter, J. E. Koglin, M. Liang, V. Mariani, A. Natan, J. Robinson, D. Rolles, A. Rudenko, K. Schnorr, H. Stapelfeldt, S. Stern, J. Thøgersen, C. H. Yoon, F. Wang, and J. Küpper, X-ray diffractive imaging of controlled gas-phase molecules: Toward imaging of dynamics in the molecular frame, *J. Comp. Phys.* **152**, 084307 (2020), arXiv:1910.13494 [physics].
- [27] P. J. Ho, D. Starodub, D. K. Saldin, V. L. Shneerson, A. Ourmazd, and R. Santra, Molecular structure determination from x-ray scattering patterns of laser-aligned symmetric-top molecules, *J. Comp. Phys.* **131**, 131101 (2009).
- [28] C. Arenz and H. Rabitz, Drawing together control landscape and tomography principles, *Physical Review A* **102**, 10.1103/physreva.102.042207 (2020).
- [29] F. Filsinger, G. Meijer, H. Stapelfeldt, H. Chapman, and J. Küpper, State- and conformer-selected beams of aligned and oriented molecules for ultrafast diffraction studies, **13**, 2076 (2011), arXiv:1009.0871 [physics].
- [30] J. Itatani, J. Levesque, D. Zeidler, H. Niikura, H. Pépin, J. C. Kieffer, P. B. Corkum, and D. M. Villeneuve, Tomographic imaging of molecular orbitals, *Nature* **432**, 867 (2004).
- [31] M. Meckel, D. Comtois, D. Zeidler, A. Staudte, D. Pavičić, H. C. Bandulet, H. Pépin, J. C. Kieffer, R. Dörner, D. M. Villeneuve, and P. B. Corkum, Laser-induced electron tunneling and diffraction, *Science* **320**, 1478 (2008).
- [32] L. Holmegaard, J. L. Hansen, L. Kalhøj, S. L. Kragh, H. Stapelfeldt, F. Filsinger, J. Küpper, G. Meijer, D. Dimitrovski, M. Abu-samaha, C. P. J. Martiny, and L. B. Madsen, Photoelectron angular distributions from strong-field ionization of oriented molecules, **6**, 428 (2010), arXiv:1003.4634 [physics].
- [33] C. J. Hensley, J. Yang, and M. Centurion, Imaging of isolated molecules with ultrafast electron pulses, *Phys. Rev. Lett.* **109**, 133202 (2012).
- [34] A. Barty, J. Küpper, and H. N. Chapman, Molecular imaging using x-ray free-electron lasers, **64**, 415 (2013).
- [35] J. Küpper, S. Stern, L. Holmegaard, F. Filsinger, A. Rouzée, A. Rudenko, P. Johnsson, A. V. Martin, M. Adolph, A. Aquila, S. Bajt, A. Barty, C. Bostedt, J. Bozek, C. Caleman, R. Coffee, N. Coppola, T. Delmas, S. Epp, B. Erk, L. Foucar, T. Gorkhovec, L. Gumprecht, A. Hartmann, R. Hartmann, G. Hauser, P. Holl, A. Hömke, N. Kimmel, F. Krasniqi, K.-U. Kühnel, J. Maurer, M. Messerschmidt, R. Moshhammer, C. Reich, B. Rudek, R. Santra, I. Schlichting, C. Schmidt, S. Schorb, J. Schulz, H. Soltau, J. C. H. Spence, D. Starodub, L. Strüder, J. Thøgersen, M. J. J. Vrakking, G. Weidenspointner, T. A. White, C. Wunderer, G. Meijer, J. Ullrich, H. Stapelfeldt, D. Rolles, and H. N. Chapman, X-ray diffraction from isolated and strongly aligned gas-phase molecules with a free-electron laser, *Phys. Rev. Lett.* **112**, 083002 (2014), arXiv:1307.4577 [physics].
- [36] J. Yang, X. Zhu, T. J. A. Wolf, Z. Li, J. P. F. Nunes, R. Coffee, J. P. Cryan, M. Gühr, K. Hegazy, T. F. Heinz, K. Jobe, R. Li, X. Shen, T. Veccione, S. Weathersby, K. J. Wilkin, C. Yoneda, Q. Zheng, T. J. Martínez, M. Centurion, and X. Wang, Imaging CF₃I conical intersection and photodissociation dynamics with ultrafast electron diffraction, *Science* **361**, 64 (2018).
- [37] S. Trippel, T. Mullins, N. L. M. Müller, J. S. Kienitz, J. J. Omiste, H. Stapelfeldt, R. González-Férez, and J. Küpper, Strongly driven quantum pendulum of the carbonyl sulfide molecule, *Phys. Rev. A* **89**, 051401(R) (2014), arXiv:1401.6897 [quant-ph].
- [38] S. Ramakrishna and T. Seideman, Rotational wavepacket imaging of molecules, *Phys. Rev. A* **87**, 023411 (2013).
- [39] F. Rosca-Pruna and M. J. J. Vrakking, Experimental observation of revival structures in picosecond laser-induced alignment of I₂, *Phys. Rev. Lett.* **87**, 153902 (2001).
- [40] A. Chatterley, E. T. Karamatskos, C. Schouder, L. Christiansen, A. V. Jørgensen, T. Mullins, J. Küpper, and H. Stapelfeldt, Switched wave packets with spectrally truncated chirped pulses, *J. Comp. Phys.* **148**, 221105 (2018), arXiv:1803.03953 [physics].
- [41] T. Kierspel, J. Wiese, T. Mullins, J. Robinson, A. Aquila, A. Barty, R. Bean, R. Boll, S. Boutet, P. Bucksbaum, H. N. Chapman, L. Christensen, A. Fry, M. Hunter, J. E. Koglin, M. Liang, V. Mariani, A. Morgan, A. Natan,

- V. Petrovic, D. Rolles, A. Rudenko, K. Schnorr, H. Stapelfeldt, S. Stern, J. Thøgersen, C. H. Yoon, F. Wang, S. Trippel, and J. Küpper, Strongly aligned molecules at free-electron lasers, **48**, 204002 (2015), arXiv:1506.03650 [physics].
- [42] E. T. Karamatskos, S. Raabe, T. Mullins, A. Trabattoni, P. Stammer, G. Goldsztejn, R. R. Johansen, K. Długołęcki, H. Stapelfeldt, M. J. J. Vrakking, S. Trippel, A. Rouzée, and J. Küpper, Molecular movie of ultrafast coherent rotational dynamics of OCS, **10**, 3364 (2019), arXiv:1807.01034 [physics].
- [43] S. Fleischer, Y. Zhou, R. W. Field, and K. A. Nelson, Molecular orientation and alignment by intense single-cycle THz pulses, *Phys. Rev. Lett.* **107**, 163603 (2011), arXiv:1105.1635 [physics].
- [44] C. T. L. Smeenk, L. Arissian, A. V. Sokolov, M. Spanner, K. F. Lee, A. Staudte, D. M. Villeneuve, and P. B. Corkum, Alignment dependent enhancement of the photoelectron cutoff for multiphoton ionization of molecules, *Phys. Rev. Lett.* **112**, 253001 (2014), arXiv:1304.6942 [physics].
- [45] C. T. L. Smeenk and P. B. Corkum, Molecular alignment using circularly polarized laser pulses, **46**, 201001 (2013).
- [46] A. Korobenko and V. Milner, Adiabatic field-free alignment of asymmetric top molecules with an optical centrifuge, *Phys. Rev. Lett.* **116**, 183001 (2016).
- [47] J. J. Larsen, K. Hald, N. Bjerre, H. Stapelfeldt, and T. Seideman, Three dimensional alignment of molecules using elliptically polarized laser fields, *Phys. Rev. Lett.* **85**, 2470 (2000).
- [48] H. Tanji, S. Minemoto, and H. Sakai, Three-dimensional molecular orientation with combined electrostatic and elliptically polarized laser fields, *Phys. Rev. A* **72**, 063401 (2005).
- [49] J. L. Hansen, L. Holmegaard, J. H. Nielsen, D. Stapelfeldt, H. and Dimitrovski, and L. B. Madsen, Orientation-dependent ionization yields from strong-field ionization of fixed-in-space linear and asymmetric top molecules, *Journal of Physics B-Atomic Molecular and Optical Physics* **45**, 015101 (2011).
- [50] A. Rouzee, S. Guerin, O. Faucher, and B. Lavorel, Field-free molecular alignment of asymmetric top molecules using elliptically polarized laser pulses, *Phys. Rev. A* **77**, 043412 (2008).
- [51] I. Nevo, L. Holmegaard, J. H. Nielsen, J. L. Hansen, H. Stapelfeldt, F. Filsinger, G. Meijer, and J. Küpper, Laser-induced 3D alignment and orientation of quantum state-selected molecules, **11**, 9912 (2009), arXiv:0906.2971 [physics].
- [52] K. Lin, I. Tutunnikov, J. Qiang, J. Ma, Q. Song, Q. Ji, W. Zhang, H. Li, F. Sun, X. Gong, H. Li, P. Lu, H. Zeng, Y. Prior, I. S. Averbukh, and J. Wu, All-optical field-free three-dimensional orientation of asymmetric-top molecules, **9**, 5134 (2018), arXiv:1803.07823 [physics].
- [53] S. S. Viftrup, V. Kumarappan, S. Trippel, H. Stapelfeldt, E. Hamilton, and T. Seideman, Holding and spinning molecules in space, *Phys. Rev. Lett.* **99**, 143602 (2007).
- [54] J. J. Larsen, I. Wendt-Larsen, and H. Stapelfeldt, Controlling the branching ratio of photodissociation using aligned molecules, *Phys. Rev. Lett.* **83**, 1123 (1999).
- [55] M. H. G. de Miranda, A. Chotia, B. Neyenhuis, D. Wang, G. Quémener, S. Ospelkaus, J. L. Bohn, J. Ye, and D. S. Jin, Controlling the quantum stereodynamics of ultracold bimolecular reactions, **7**, 502–507 (2011).
- [56] K. P. Liu, Crossed-beam studies of neutral reactions: State-specific differential cross sections, **52**, 139 (2001).
- [57] Y. Shagam, A. Klein, W. Skomorowski, R. Yun, V. Averbukh, C. P. Koch, and E. Narevicius, Molecular hydrogen interacts more strongly when rotationally excited at low temperatures leading to faster reactions, **7**, 921 (2015).
- [58] M. Leibscher, I. Averbukh, and H. Rabitz, Molecular alignment by trains of short laser pulses, *Phys. Rev. Lett.* **90**, 213001 (2003).
- [59] C. Cornaggia, Electronic dynamics of charge resonance enhanced ionization probed by laser-induced alignment in C₂H₂, **49**, 19LT01 (2016).
- [60] E. Hamilton, T. Seideman, T. Ejdrup, M. D. Poulsen, C. Z. Bisgaard, S. S. Viftrup, and H. Stapelfeldt, Alignment of symmetric top molecules by short laser pulses, *Phys. Rev. A* **72**, 043402 (2005).
- [61] E. Péronne, M. D. Poulsen, H. Stapelfeldt, C. Z. Bisgaard, E. Hamilton, and T. Seideman, Nonadiabatic laser-induced alignment of iodobenzene molecules, *Phys. Rev. A* **70**, 063410 (2004).
- [62] J. P. Cryan, P. H. Bucksbaum, and R. N. Coffee, Field-free alignment in repetitively kicked nitrogen gas, *Phys. Rev. A* **80**, 063412 (2009).
- [63] J. J. Larsen, H. Sakai, C. P. Safvan, I. Wendt-Larsen, and H. Stapelfeldt, Aligning molecules with intense non-resonant laser fields, *J. Comp. Phys.* **111**, 7774 (1999).
- [64] O. Ghafur, A. Rouzée, A. Gijbsbertsen, W. K. Siu, S. Stolte, and M. J. J. Vrakking, Impulsive orientation and alignment of quantum-state-selected NO molecules, **5**, 289 (2009).
- [65] L. Holmegaard, J. H. Nielsen, I. Nevo, H. Stapelfeldt, F. Filsinger, J. Küpper, and G. Meijer, Laser-induced alignment and orientation of quantum-state-selected large molecules, *Phys. Rev. Lett.* **102**, 023001 (2009), arXiv:0810.2307 [physics].
- [66] K. Hoshina, K. Yamanouchi, T. Ohshima, Y. Ose, and H. Todokoro, Alignment of cs₂ in intense nanosecond laser fields probed by pulsed gas electron diffraction, *J. Comp. Phys.* **118**, 6211 (2003).
- [67] J. H. Nielsen, P. Simesen, C. Z. Bisgaard, H. Stapelfeldt, F. Filsinger, B. Friedrich, G. Meijer, and J. Küpper, Stark-selected beam of ground-state OCS molecules characterized by revivals of impulsive alignment, **13**, 18971 (2011), arXiv:1105.2413 [physics].
- [68] D. W. Broege, R. N. Coffee, and P. H. Bucksbaum, Strong-field impulsive alignment in the presence of high temperatures and large centrifugal distortion, *Phys. Rev. A* **78**, 035401 (2008).
- [69] G. Galinis, L. G. Mendoza Luna, M. J. Watkins, A. M. Ellis, R. S. Minns, M. Mladenovic, M. Lewerenz, R. T. Chapman, I. C. E. Turcu, C. Cacho, E. Springate, L. Kazak, S. Gode, R. Irsig, S. Skruszewicz, J. Tiggesbaumker, K.-H. Meiwes-Broer, A. Rouzee, J. G. Underwood, M. Siano, and K. von Haeften, Formation of coherent rotational wavepackets in small molecule-helium clusters using impulsive alignment, **171**, a95 (2014).
- [70] S. Guérin, A. Rouzée, and E. Hertz, Ultimate field-free molecular alignment by combined adiabatic-impulsive field design, *Phys. Rev. A* **77**, 041404 (2008).
- [71] J. S. Kienitz, S. Trippel, T. Mullins, K. Długołęcki, R. González-Férez, and J. Küpper, Adiabatic mixed-field orientation of ground-state-selected carbonyl sulfide molecules, *Comp. Phys. Comm.* **17**, 3740 (2016), arXiv:1607.05615 [physics].

- [72] J. J. Omiste, M. Gaertner, P. Schmelcher, R. González-Férez, L. Holmegaard, J. H. Nielsen, H. Stapelfeldt, and J. Küpper, Theoretical description of adiabatic laser alignment and mixed-field orientation: the need for a non-adiabatic model, **13**, 18815 (2011), arXiv:1105.0534 [physics].
- [73] J. J. Omiste and R. González-Férez, Theoretical description of the mixed-field orientation of asymmetric-top molecules: A time-dependent study, *Physical Review A* **94**, 10.1103/physreva.94.063408 (2016).
- [74] H. Stapelfeldt and T. Seideman, Colloquium: Aligning molecules with strong laser pulses, *Rev. Mod. Phys.* **75**, 543 (2003).
- [75] L. Holmegaard, S. S. Viftrup, V. Kumarappan, C. Z. Bisgaard, H. Stapelfeldt, E. Hamilton, and T. Seideman, Control of rotational wave-packet dynamics in asymmetric top molecules, *Phys. Rev. A* **75**, 051403 (2007).
- [76] T. Seideman, Revival structure of aligned rotational wave packets, *Phys. Rev. Lett.* **83**, 4971 (1999).
- [77] R. Damari, S. Kallush, and S. Fleischer, Rotational control of asymmetric molecules: Dipole- versus polarizability-driven rotational dynamics, *Phys. Rev. Lett.* **117**, 103001 (2016).
- [78] M. Artamonov and T. Seideman, Three-dimensional laser alignment of polyatomic molecular ensembles, **110**, 885 (2012).
- [79] P. W. Joireman, L. L. Connell, S. M. Ohline, and P. M. Felker, Characterization of asymmetry transients in rotational coherence spectroscopy, *J. Comp. Phys.* **96**, 4118 (1992).
- [80] P. M. Felker, J. S. Baskin, and A. H. Zewail, Rephasing of collisionless molecular rotational coherence in large molecules, *J. Phys. Chem.* **90**, 724 (1986).
- [81] L. L. Connell, S. M. Ohline, P. W. Joireman, T. C. Corcoran, and P. M. Felker, Rotational coherence spectroscopy of 1-naphthol-(water)₂ clusters: Structural evidence for a cyclic hydrogen-bonded trimer, *J. Comp. Phys.* **94**, 4668 (1991).
- [82] J. Maurer, D. Dimitrovski, L. Christensen, L. B. Madsen, and H. Stapelfeldt, Molecular-frame 3D photoelectron momentum distributions by tomographic reconstruction, *Phys. Rev. Lett.* **109**, 123001 (2012).
- [83] M. Graus, C. Metzger, M. Grimm, P. Nigge, V. Feyer, A. Schöll, and F. Reinert, Three-dimensional tomographic imaging of molecular orbitals by photoelectron momentum microscopy, *The European Physical Journal B* **92**, 10.1140/epjb/e2019-100015-x (2019).
- [84] S. Zhdanovich, A. A. Milner, C. Bloomquist, J. Floß, I. Sh. Averbukh, J. W. Hepburn, and V. Milner, Control of molecular rotation with a chiral train of ultrashort pulses, *Phys. Rev. Lett.* **107**, 243004 (2011).
- [85] V. Milner and J. W. Hepburn, Laser control of ultrafast molecular rotation, **159**, 395 (2016).
- [86] A. Milner, A. Korobenko, and V. Milner, Field-free long-lived alignment of molecules with a two-dimensional optical centrifuge, *Phys. Rev. A* **93**, 053408 (2016).
- [87] A. Owens, A. Yachmenev, S. N. Yurchenko, and J. Küpper, Climbing the Rotational Ladder to Chirality, *Phys. Rev. Lett.* **121**, 193201 (2018), arXiv:1802.07803 [physics].
- [88] L. Yuan, S. W. Teitelbaum, A. Robinson, and A. S. Mullin, Dynamics of molecules in extreme rotational states, *Proc. Nat. Acad. Sci. USA* **108**, 6872 (2011).
- [89] Y. Khodorkovsky, U. Steinitz, J.-M. Hartmann, and I. Sh. Averbukh, Collisional dynamics in a gas of molecular super-rotors, **6**, 7791 (2015).
- [90] A. A. Milner, A. Korobenko, J. W. Hepburn, and V. Milner, Effects of ultrafast molecular rotation on collisional decoherence, *Phys. Rev. Lett.* **113**, 043005 (2014).
- [91] A. A. Milner, A. Korobenko, K. Rezaiezhadeh, and V. Milner, From gyroscopic to thermal motion: A crossover in the dynamics of molecular superrotors, **5**, 031041 (2015).
- [92] E. Zak, A. Yachmenev, and J. Kupper, Controlling rotation in the molecular-frame with an optical centrifuge, submitted (2021).
- [93] A. Owens, A. Yachmenev, and J. Küpper, Coherent control of the rotation axis of molecular superrotors, **9**, 4206 (2018), arXiv:1807.04016 [physics].
- [94] M. S. Ashbaugh, C. C. Chicone, and R. H. Cushman, The twisting tennis racket, *Journal of Dynamics and Differential Equations* **3**, 67 (1991).
- [95] B. Zhilinskii, I. Kozin, and S. Petrov, Correlation between asymmetric and spherical top: imperfect quantum bifurcations, *Spectrochimica Acta Part A: Molecular and Biomolecular Spectroscopy* **55**, 1471 (1999).
- [96] K. Hamraoui, L. V. Damme, P. Mardešić, and D. Sugny, Classical and quantum rotation numbers of asymmetric-top molecules, *Physical Review A* **97**, 10.1103/physreva.97.032118 (2018).
- [97] L. V. Damme, D. Leiner, P. Mardesic, S. J. Glaser, and D. Sugny, Linking the rotation of a rigid body to the schrödinger equation: The quantum tennis racket effect and beyond, *Scientific Reports* **7**, 10.1038/s41598-017-04174-x (2017).
- [98] Y. Ma, K. E. Khosla, B. A. Stickler, and M. Kim, Quantum persistent tennis racket dynamics of nanorotors, *Physical Review Letters* **125**, 10.1103/physrevlett.125.053604 (2020).
- [99] E. Zak, A. Yachmenev, and J. Kupper, Creating, controlling and detecting dynamic chirality, submitted (2021).
- [100] M. Lapert, S. Guérin, and D. Sugny, Field-free quantum cogwheel by shaping of rotational wave packets, *Phys. Rev. A* **83**, 013403 (2011).
- [101] A. Korobenko, J. W. Hepburn, and V. Milner, Observation of nondispersing classical-like molecular rotation, **17**, 951 (2015).
- [102] C. P. Koch, M. Lemeshko, and D. Sugny, Quantum control of molecular rotation, *Rev. Mod. Phys.* **91**, 035005 (2019).
- [103] S. Kerbstadt, E. Zak, J. Küpper, *et al.*, please add, in preparation (2020).
- [104] S. N. Yurchenko, W. Thiel, and P. Jensen, Theoretical ROVibrational Energies (TROVE): A robust numerical approach to the calculation of rovibrational energies for polyatomic molecules, **245**, 126 (2007).
- [105] A. Yachmenev and S. N. Yurchenko, Automatic differentiation method for numerical construction of the rotational-vibrational Hamiltonian as a power series in the curvilinear internal coordinates using the Eckart frame, *J. Comp. Phys.* **143**, 014105 (2015).
- [106] S. N. Yurchenko, A. Yachmenev, and R. I. Ovsyannikov, Symmetry adapted ro-vibrational basis functions for variational nuclear motion calculations: TROVE approach, **13**, 4368 (2017), arXiv:1708.07185 [physics].
- [107] A. A. A. Azzam, J. Tennyson, S. N. Yurchenko, and O. V. Naumenko, ExoMol molecular line lists – XVI. the rotation–vibration spectrum of hot H₂S, **460**, 4063

- (2016).
- [108] A. Owens and A. Yachmenev, RichMol: A general variational approach for rovibrational molecular dynamics in external electric fields, *J. Comp. Phys.* **148**, 124102 (2018), arXiv:1802.07603 [physics].
- [109] A. Yachmenev, L. V. Thesing, and J. Küpper, Laser-induced dynamics of molecules with strong nuclear quadrupole coupling, *J. Comp. Phys.* **151**, 244118 (2019), arXiv:1910.13275 [physics].
- [110] R. D. Johnson, III, ed., *NIST Computational Chemistry Comparison and Benchmark Database* (NIST Standard Reference Database Number 101, Release 20, 2019).
- [111] M. Artamonov and T. Seideman, Theory of three-dimensional alignment by intense laser pulses, *The Journal of Chemical Physics* **128**, 154313 (2008).
- [112] S. S. Viftrup, V. Kumarappan, L. Holmegaard, C. Z. Bisgaard, H. Stapelfeldt, M. Artamonov, E. Hamilton, and T. Seideman, Controlling the rotation of asymmetric top molecules by the combination of a long and a short laser pulse, *Phys. Rev. A* **79**, 023404 (2009).
- [113] I. F. Tenney, M. Artamonov, T. Seideman, and P. H. Bucksbaum, Collisional decoherence and rotational quasirevivals in asymmetric-top molecules, *Physical Review A* **93**, 10.1103/physreva.93.013421 (2016).
- [114] J. Ortigoso, Design of tailored microwave pulses to create rotational coherent states for an asymmetric-top molecule, *Physical Review A* **57**, 4592 (1998).
- [115] J. Salomon, C. M. Dion, and G. Turinici, Optimal molecular alignment and orientation through rotational ladder climbing, *The Journal of Chemical Physics* **123**, 144310 (2005).
- [116] L. H. Coudert, Optimal control of the orientation and alignment of an asymmetric-top molecule with terahertz and laser pulses, *The Journal of Chemical Physics* **148**, 094306 (2018).